

Supporting Information for

## **Lasing Action with Gold Nanorod Hyperbolic Metamaterials**

*Rohith Chandrasekar<sup>1</sup>, Zhuoxian Wang<sup>1</sup>, Xiangeng Meng<sup>1,\*</sup>, Shaimaa I. Azzam<sup>1</sup>, Mikhail Y. Shalaginov<sup>1</sup>, Alexei Lagutchev<sup>1</sup>, Young L. Kim<sup>2</sup>, Alexander Wei<sup>3</sup>, Alexander V. Kildishev<sup>1</sup>, Alexandra Boltasseva<sup>1</sup>, and Vladimir M. Shalaev<sup>1,\*</sup>*

<sup>1</sup>School of Electrical and Computer Engineering and Birck Nanotechnology Center, Purdue University, West Lafayette, IN 47907, USA

<sup>2</sup>School of Biomedical Engineering, Purdue University, West Lafayette, IN 47907, USA

<sup>3</sup>Department of Chemistry, Purdue University, West Lafayette, IN 47907, USA

## S1. Fabrication and characterization

The arrays were fabricated by anodizing 250 nm thick aluminum films deposited on glass substrates with 15 nm thick tantalum pentoxide and 5 nm thick gold under layers. All layers were deposited using an electron-beam evaporator (Leybold, Inc). The films were anodized in 0.3 M  $\text{H}_2\text{SO}_4$  at 1°C until the aluminum film was fully anodized. Substrate anodization was performed at 30 V for the HMM cavity and at 25 V for the EMM cavity. A solution of 30 mM sodium hydroxide was used to remove the alumina barrier layer as well as widen the pores. For the HMM, the pores were widened for 60 s, while they were widened only for 25 s for the EMM. This fabrication procedure yielded HMM and EMM alumina templates with approximate pore diameters and surface densities of 40 nm and 35% and 25 nm and 14%, respectively (Figure S1).

Gold nanorods were grown to the full thickness of the template (~250 nm) by electrodeposition using Orotemp Gold Electrolyte (Technic Inc.) with a constant current of 0.5 mA/cm<sup>2</sup> using a Princeton Research Systems power supply, at which point a distinct drop in voltage (> 20%) was observed. Samples were then cleaned using acetone, isopropanol and DI water and were dried under gentle nitrogen stream.

Transmission spectra were taken using a variable-angle spectroscopic ellipsometer (J.A. Woollam & Co.). SEM images are taken with a Hitachi Field-Emission Scanning Electron Microscope.

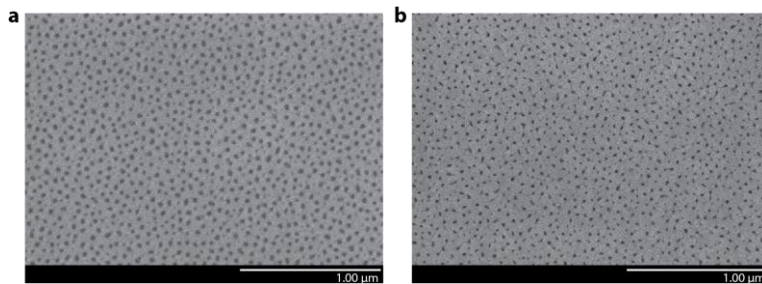


Figure S1. SEM images of alumina templates for (a) HMM and (b) EMM.

## S2. Simulations of nanorod metamaterials

We calculate the extinction spectra of the HMM and EMM for  $0^\circ$ ,  $20^\circ$ , and  $40^\circ$  incidence using CST Microwave Studio. The simulated domain, unit cell as well as experimental and simulated extinction spectra are shown in Figure S2.

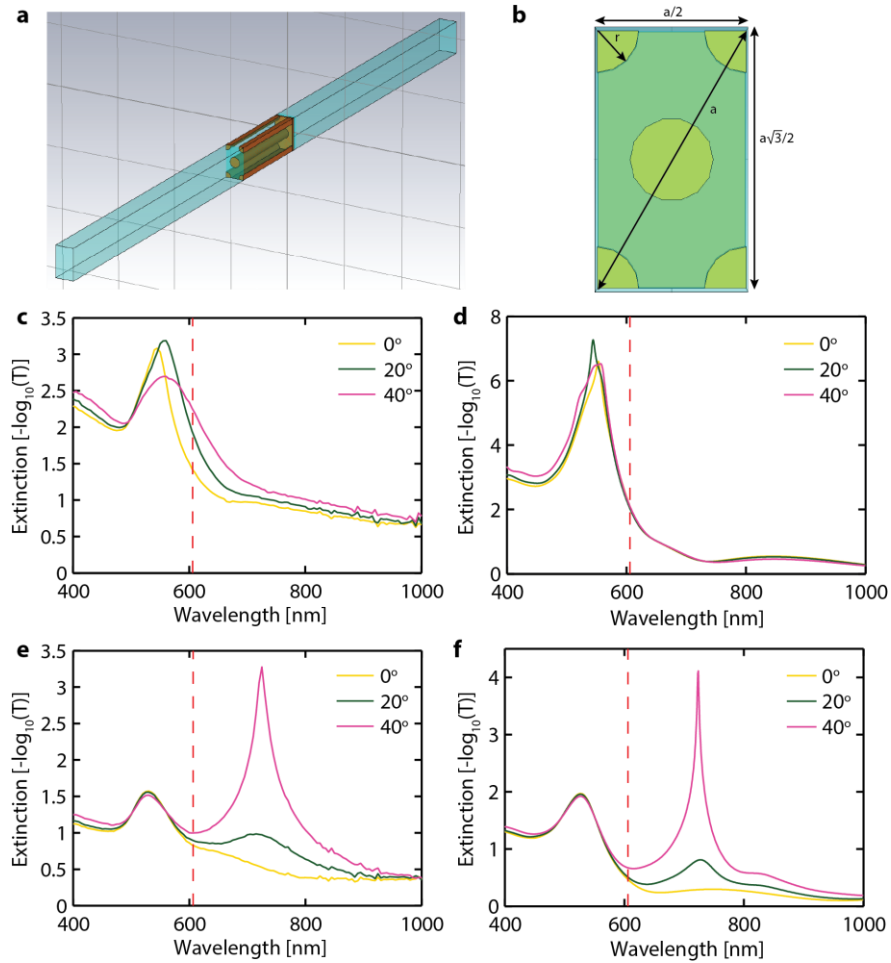


Figure S2. (a) Simulation domain, (b) unit cell of structure, (c, e) experimental extinction spectra of HMM (c) and EMM (e), simulated extinction spectra of HMM (d) and EMM (f). Red dashed line indicates the central emission wavelength from R101 (606 nm).

The structure, shown in Figure S2a, comprises of a 1- $\mu\text{m}$  glass substrate ( $\epsilon = 2.25$ ), covered with 15-nm tantalum pentoxide ( $\epsilon = 4.2$ ) and 5-nm gold layers. The gold nanorods have radius of  $r$ , and are 250 nm in length. The superstrate is air, and is 1  $\mu\text{m}$  in length. The unit cell of the structure, shown in Figure S2b, has a diagonal length of  $a$ , and hence top width of  $a/2$  and side length of  $a\sqrt{3}/2$ . For both, the EMM and HMM models, the diagonal length  $a$  is 120 nm. For the EMM, the rod diameter is 23.5 nm, yielding a metal fill ratio ( $f$ ) of about 14%. The HMM has the rod with a diameter of 38 nm, which gives a metal fill ratio ( $f$ ) of about 35%. The alumina host has a refractive index of 1.77. The dispersion of gold is defined by a Drude term plus 2 critical points fitted to the Johnson-Christy data, with a loss factor of 2 [1-2]. The experimental extinction spectra for the HMM and EMM samples are shown in Figures S2c,e and the simulated fits are shown in Figures S2d,f respectively. While the spectral features of the experimental curves are similar to the simulated ones, the simulated curves certainly show much sharper resonances. This discrepancy is mostly due to imperfection of samples, i.e. roughness of the nanorods and alumina membrane, as well as inhomogeneity of the nanorods, which would cause inhomogeneous broadening.

### S3. Iso-frequency curves of nanorod metamaterials

We have calculated the iso-frequency curves (Equation 1 below) for 250 nm thick nanorod metamaterial slabs with 35% (HMM) and 14% (EMM) metal fill ratios, as shown in Figure S3. The nanorod metamaterials have been simulated using local effective medium theory.  $k_{||}$  is the in-plane wavevector, and  $k_{\perp,\text{eff}}$  is the effective wavevector of the propagating modes in the nanorod metamaterial. The iso-frequency curves confirms the hyperbolic and elliptic dispersion at 606 nm for HMM and EMM samples, respectively.

$$\frac{k_{\perp,\text{eff}}}{k_0} = \pm \sqrt{\epsilon_{||} \left( 1 - \frac{(k_{||}/k_0)^2}{\epsilon_{\perp}} \right)}, \quad (1)$$

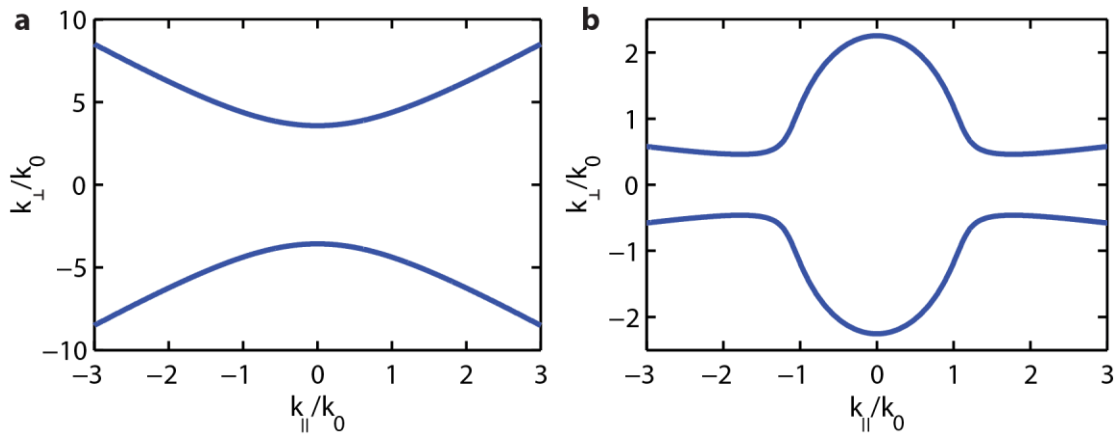


Figure S3. Iso-frequency curves at 606 nm for HMM (a) and EMM (b).

#### S4. Simulations of plasmonic modes in nanorod metamaterials

In order to further study the decay channels providing the Purcell enhancement in HMM and EMM, we have also calculated the inherent plasmonic modes (often named as high-k modes) that can be excited in our HMM and EMM structures. Figure S4 shows the k-space dissipated power density,  $\log_{10}[k_0 dF_p^{ave}/dk_{\parallel}]$ , calculated for a dipole with the averaged orientation, located 20 nm above the surface of HMM and EMM, defined by local EMT. The formulas used for the calculation of the k-space dissipated power density are [3]

$$\frac{dF_p^{\perp}}{ds} = \frac{3}{2} \operatorname{Re} \left\{ \frac{s^3}{s_{\perp, \text{sup}}(s) \epsilon_{\text{sup}}^{3/2}} (1 + \tilde{r}^p(s) e^{2ik_0 s_{\perp, \text{sup}}(s) h}) \right\}$$

$$\frac{dF_p^{\parallel}}{ds} = \frac{3}{4} \frac{1}{\epsilon_{\text{sup}}^{1/2}} \operatorname{Re} \left\{ \frac{s}{s_{\perp, \text{sup}}(s)} \left[ 1 + \frac{s_{\perp, \text{sup}}^2(s)}{\epsilon_{\text{sup}}} + \left( \tilde{r}^s(s) - \frac{s_{\perp, \text{sup}}^2(s)}{\epsilon_{\text{sup}}} \tilde{r}^p(s) \right) e^{2ik_0 s_{\perp, \text{sup}}(s) h} \right] \right\}$$

$$\frac{dF_p^{ave}}{ds} = \frac{1}{3} \frac{dF_p^{\perp}}{ds} + \frac{2}{3} \frac{dF_p^{\parallel}}{ds}$$

Where  $s = \frac{k_{\parallel}}{k_0}$ ,  $s_{\perp, \text{sup}}(s) = \frac{k_{\perp, \text{sup}}(s)}{k_0} = (\epsilon_{\text{sup}} - s^2)^{1/2}$ .

The Fresnel reflection coefficients for p- and s-polarized light  $\tilde{r}^p$  and  $\tilde{r}^s$  were calculated using analogue of the Drude formula [4].

In both HMM and EMM, we can see the modal gap, i.e., wavelength range where very few plasmonic modes are allowed between ENP and ENZ resonances. We see that at 606 nm, EMM falls in this modal gap with almost no propagating modes, while HMM provides a vast amount of modes to enhance the emitter's decay rate, for even very large  $k_{\parallel}$  (in-plane wavevector). Due to this large number of allowed modes, we clearly see that the HMM structure provides significant Purcell enhancement over the EMM structure, and is therefore expected to enhance spontaneous emission greatly, which in turn could feed into lasing modes.

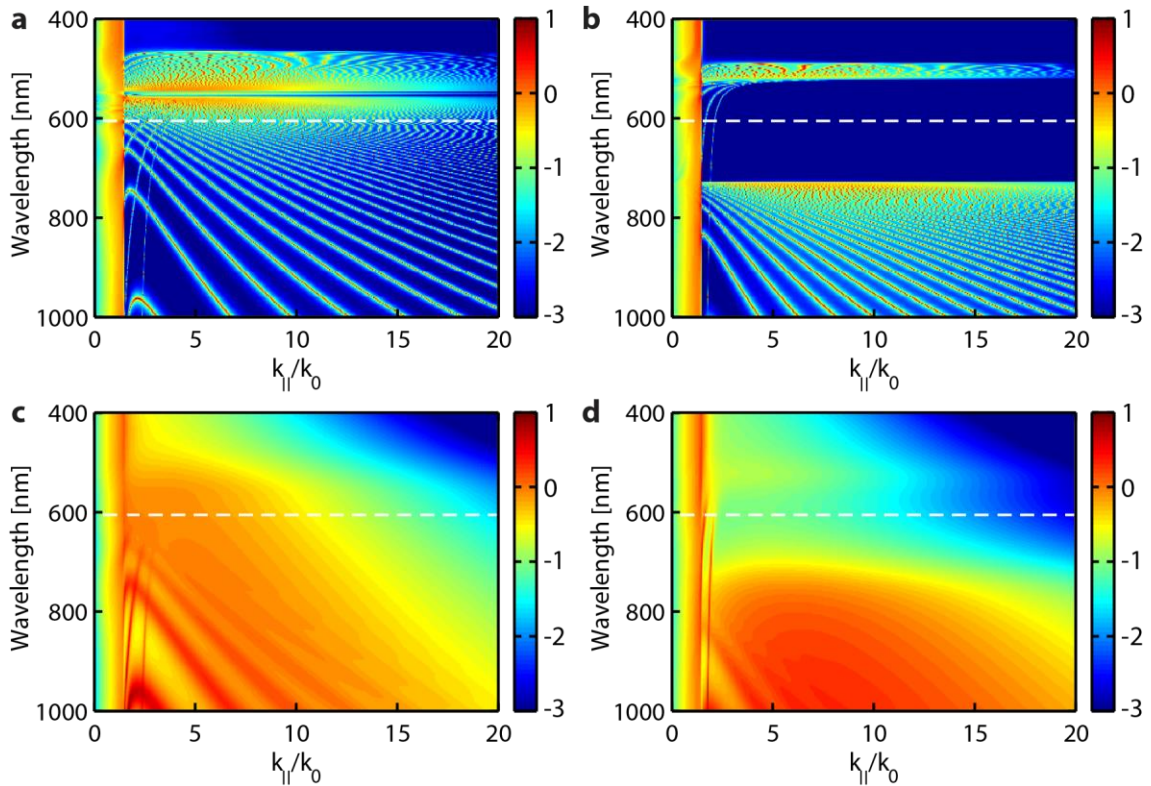


Figure S4. k-space dissipated power density for a dipole placed 20 nm above HMM (a) and EMM (b), without considering losses. (c) and (d) correspond to the cases of (a) and (b) with actual losses. At 606 nm (white dotted line), HMM provides many more inherent plasmonic modes than EMM. The white dashed lines indicate the position of the central emission wavelength of R101 (606 nm).

## S5. Lasing experiments

The nanorod arrays are spin coated with a 10 mM solution of R101 dye dissolved in PVA at 1000 rpm for 30 s followed by baking at 60 °C for 6 hours, which yields a  $\sim 2$   $\mu\text{m}$ -thick film. A frequency-doubled Nd:YAG picosecond laser (532 nm, 400 ps pulse width, and 1 Hz repetition rate) is used to pump the samples at 40°, as shown in Figure S5. The pump pulses are focused down to a spot size of  $\sim 200$   $\mu\text{m}$  in diameter using a 5 $\times$  objective lens. The emission from the samples is collected with a fiber almost normal to the sample surface, which is fed to a spectrometer (SP-2150i, Princeton Instruments) equipped with a charge-coupled device (CCD).

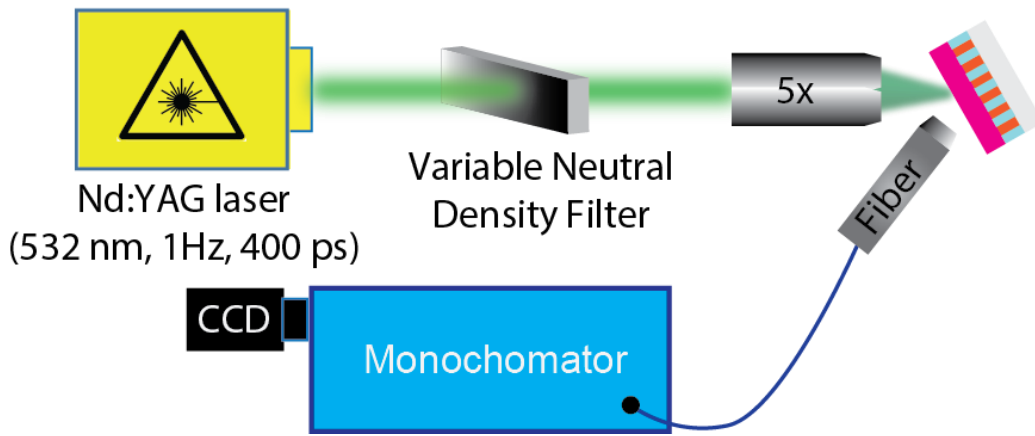


Figure S5. Schematic of the experimental setup used to collect lasing emission from nanorod metamaterial samples.

## S6. Spectral narrowing and threshold distribution for nanorod HMM and EMM

One proof of lasing action is a significant reduction in the full width at half maximum (FWHM) of the emission spectra as the pump energy is increased. The FWHM for the emission spectra of nanorod HMM and EMM are shown below in Figure S6. The linewidth of the lasing emission from the nanorod HMM is reduced from  $\sim 24$  nm to  $\sim 6$  nm as the pump energy is increased to above the threshold. This linewidth is comparable to various other demonstrated lasing systems using dyes as gain media. For the nanorod EMM, we also see a reduction of the linewidth. We see the reduction in FWHM for the HMM at lower pump energy as compared to EMM, hence exhibiting lower threshold.

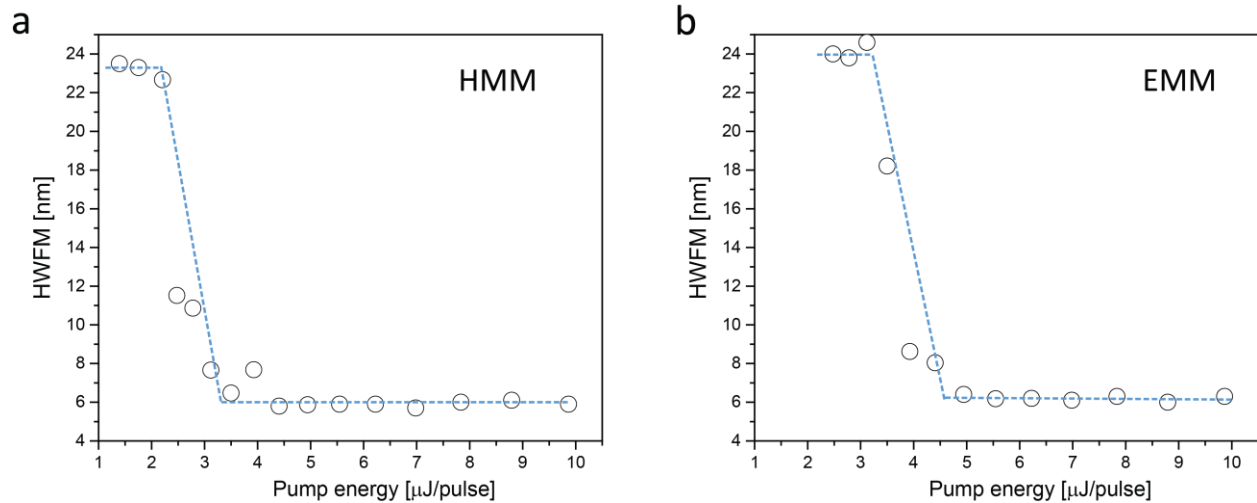


Figure S6. Spectral linewidth of the emission as a function of the pump energy for nanorod HMM (a) and EMM (b) samples, respectively.

### S7. Threshold distribution for nanorod HMM and EMM

We have studied the threshold behavior for nanorod HMM and EMM samples at 5 different points from each sample. The distribution of threshold values for both samples is shown below in Figure S7. We see that on average the HMM gives us a reduction of  $\sim 35\%$  in threshold compared to the EMM sample.

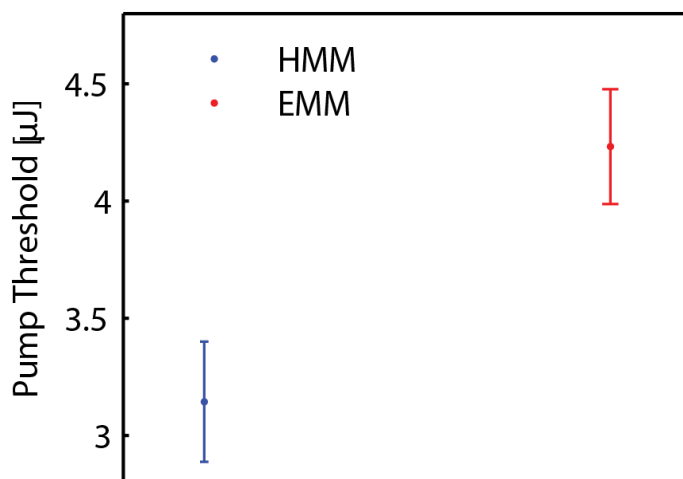


Figure S7. The average pump thresholds of HMM and EMM samples respectively, obtained by measuring five different points from each sample.

## S8. Emission measurements with control samples

We measured the emission from a bare glass substrate and 250 nm thick gold film deposited on glass, both coated with a 2- $\mu\text{m}$  layer of PVA embedded with R101 where the concentration of R101 is 10 mM relative to PVA. The results are shown in Figure S8 below. Both samples exhibit broadband emission, but show no lasing peaks.

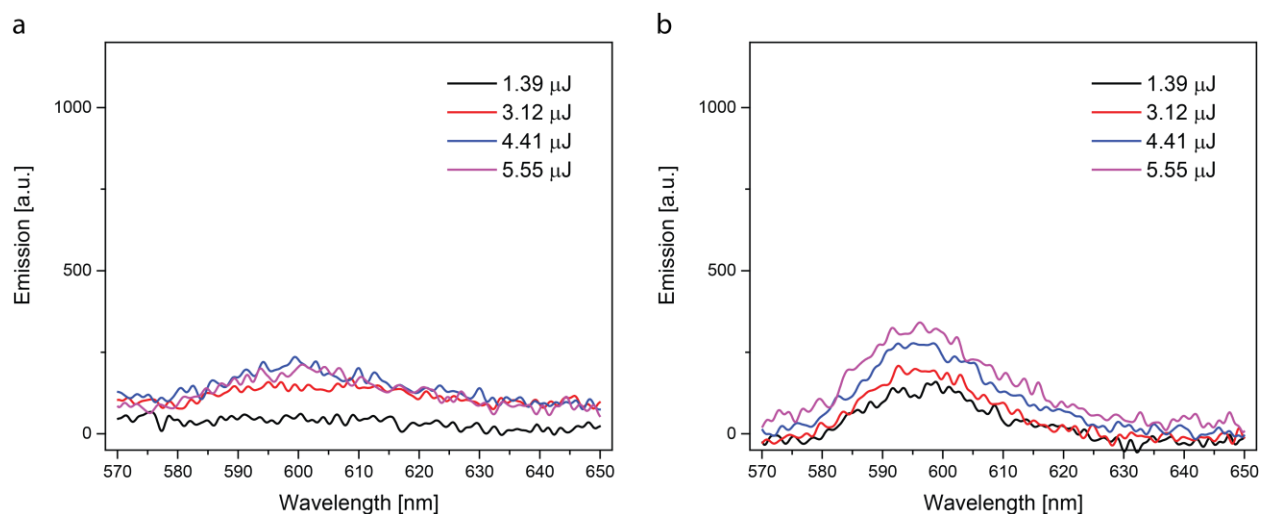


Figure S8. Emission measurements from (a) glass substrate and (b) 250 nm gold film on glass samples coated with a 2- $\mu\text{m}$  layer of R101 embedded in PVA.

## S9. Emission from lamellar HMM sample

We measured the emission from a lamellar metal-dielectric stack of alumina and gold layers coated with R101 in PVA. The structure is composed of 10 pairs of a 8.9 nm thick gold layer and a 16.1 nm thick alumina layer, which has the same thickness (250 nm) and metal fill ratio (~35%) as the nanorod HMM. The emission measurements are shown in Figure S9a. The plots only shows spontaneous emission and no lasing peaks are observed. We have also quantitatively compared the emission intensity from lamellar and nanorod HMMs, shown in Figure S9b. We can see that the emission from nanorod HMM increases more rapidly than that from lamellar HMM, although the emission intensity from the latter is stronger than the former at low pump energy.

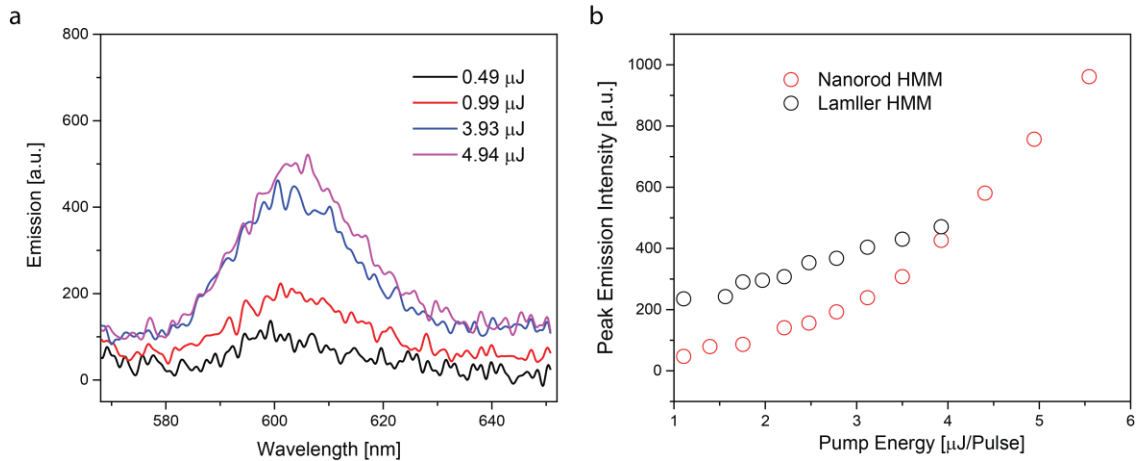


Figure S9. (a) Emission from Lamellar HMM composed on 10 pairs of 8.9 nm gold film and 16.1 nm alumina film, coated with R101 in PVA. Plots show only broad spontaneous emission bands. (b) Comparison of emission intensity from nanorod and lamellar HMMs.

## S10. Local mode and field distributions

The mode and field distributions of gold nanorod metamaterials are calculated using 3D full-wave numerical simulations with a commercial finite-element solver (COMSOL Multiphysics 5.2a, Wave Optics Module). The simulated domains are set as reported in Reference 5. The material properties are as provided in section S2.

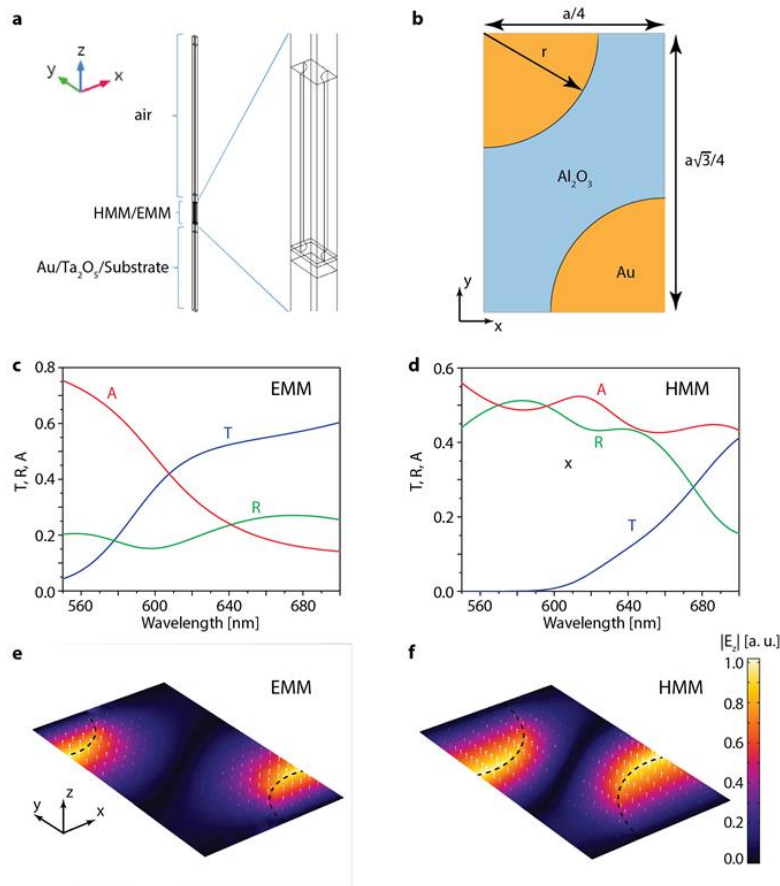


Figure S10. (a) Simulation domain, (b) unit cell of structure, (c,d) calculated optical spectra of EMM (c) and HMM (d): transmission (blue), reflection (green), and absorption (red), (e,f)  $|E_z|$  field distribution of the unit cell shown in (b) for EMM (e) and HMM (f). The dashed lines indicate the position of the nanorod. The magnitude of  $|E_z|$  field is normalized with respect to the maximum value that is the same for HMM and EMM.

## **S11 Finite-difference time-domain (FDTD) simulations showing lasing behavior in HMM and EMM laser devices**

Lasing action in HMM and EMM laser devices have been modeled using a four-level atomic system [2] incorporated in a commercial FDTD solver (Lumerical, FDTD Solutions) [6]. The induced polarizations due to transitions between different levels are coupled to Maxwell equations, which are solved in time domain to obtain the emission from lasing at 606 nm. The parameters of Rhodamine 101 dye used in the simulations were obtained by fitting the experimental transmission data [7]. Lasing behavior is clearly observed in our simulations as depicted in Figure S11a showing the spectral linewidth narrowing and Figures S11b,c showing “S” shape dependence of the power output versus the pump energy. The pump thresholds for lasing obtained from simulations are around 0.8  $\mu\text{J}$  for HMM and 1.5  $\mu\text{J}$  for EMM, which are within one order magnitude of what we observed in our experiments.

Furthermore, our simulation results are fitted using the rate equations [8].

$$\frac{dn}{dt} = \sigma p - An - \Gamma As(n - n_0)$$

$$\frac{ds}{dt} = \beta An + \Gamma As(n - n_0) - \gamma s$$

where  $s$  is the photon density,  $n$  is the exciton density and  $p$  is the pump rate. The incident pump pulse takes the form  $p(t) = p_0 \exp\left(-\frac{t-t_0}{\delta t}\right)^2$ , where the pulse width  $\delta t = 1$  ps. In such a simplified analysis, we have assumed rapid ground level depletion,  $n_0 = 0$ , a mode confinement factor,  $\Gamma = 1$  and a pump photon to laser photon conversion efficiency,  $\sigma = 1$ .

The fitted parameters are the exciton lifetime,  $A^{-1}$ , the photon lifetime in the cavity,  $\gamma^{-1}$  and the spontaneous emission factor,  $\beta$ . For HMM sample, the best fitted parameters are found to be  $A^{-1} = 2$  ns,  $\gamma^{-1} = 1$  fs and  $\beta = 0.23$  (Figure S11b).  $\gamma$  is defined by the losses from both decoherence in the dye  $\gamma_d = 25.5$  fs<sup>-1</sup> and the losses from plasmonic mode providing the feedback for lasing, found to be  $\gamma_f = 1.04$  fs<sup>-1</sup>. For EMM, the best fitted parameters are  $A^{-1} = 2$  ns,  $\gamma^{-1} = 1.5$  fs and  $\beta = 0.08$  (Figure S11c). The  $\beta$  of EMM is significant smaller than that of HMM indicating a smaller portion of spontaneous emission is coupled into lasing mode in EMM.

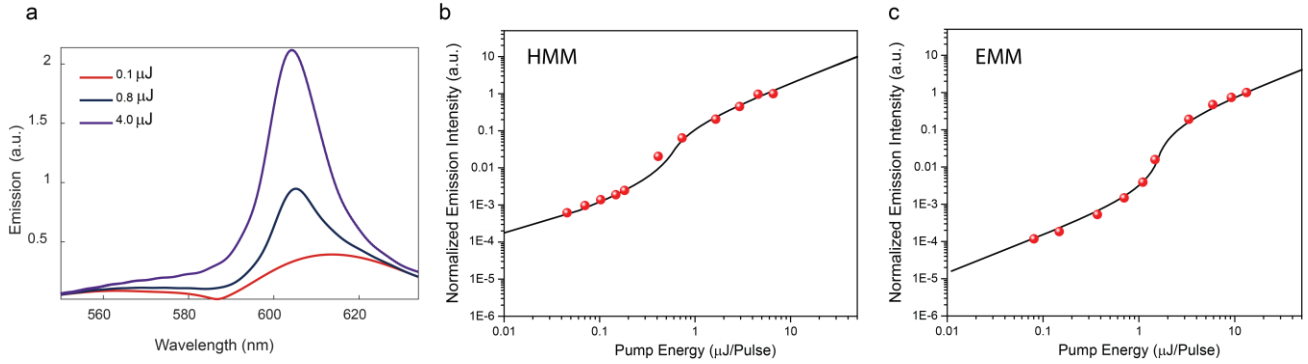


Figure S11. (a) Emission spectra at different pump energies from the HMM laser device. Spectral linewidth narrowing is observed when the pump energy reaches the threshold ( $\sim 0.8\mu\text{J}$ ). (b-c) Normalized emission intensity as a function of the pump energy showing “S” shape behavior for HMM (b) and EMM (c), respectively. The red dots represent the results from our FDTD simulations, while the solid curves indicate the results from fitting with the rate equations.

## References

- [1] Ni, X., Liu, Z., Kildishev, A. V. *PhotonicsDB: Optical Constants*, **2015**, <https://nanohub.org/resources/PhotonicsDB>. (DOI: 10.4231/D35H7BV58).
- [2] Prokopeva, L J.; Trieschmann, J; Klar, T. A.; Kildishev, A. V. "Numerical modeling of active plasmonic metamaterials." In SPIE Optical Systems Design, pp. 81720B-81720B. International Society for Optics and Photonics, **2011**.
- [3] Novotny, L.; Hecht, B., *Principles of Nano-Optics*. Cambridge University press: **2012**.
- [4] Drude, P. *Ann. Phys.* **1889**, 282, 865.
- [5] Lyvers, D. P.; Moon, J.; Kildishev, A. V.; Shalaev, V. M.; Wei, A. *ACS Nano* **2008**, 2, 2569-2576.
- [6] Lumerical Solutions, Inc. <http://www.lumerical.com/tcad-products/fdtd/>
- [7] Fang, J.; Liu, J.; Wang, Z.; Meng, X.; Prokopeva, L.; Shalaev, V. M.; Kildishev, A. V., "Time-Domain Model of 4-Level Gain System Fitted to Nanohole Array Lasing Experiment." In CLEO: QELS\_Fundamental Science, pp. FW3E-5. Optical Society of America, **2015**.
- [8] Yokoyama, H. and Brorson, S.D. *J. Appl. Phys.*, **1989**, 66, 4801-4805.